Materials LAB

RESEARCH ARTICLE

Materials Lab 2025, 4, 250103

Effects of mechanical vibration on the solidification microstructure and properties of Cu-*x*Sn alloys

Huikun Wang[1], Jia Sun[1], Jian Zhang[2], Mingfei Wang[1], Bo Peng[1*], Guangxu Dong[1], Tingju Li[1,3] and Jinchuan Jie[1,3*]

This study prepared Cu-*x*Sn (wt.%) alloys using intermediate-frequency induction heating coupled with a mechanical vibration (MV) field, followed by comprehensive microstructural characterization and property evaluations. Characterization techniques such as X-ray diffractometer (XRD), scanning electron microscope (SEM), and electron probe microanalyzer (EPMA) were employed to analyze the phase composition and distribution of the Cu-*x*Sn alloys. The experimental results show that the macroscopic solidification structure of the Cu-*x*Sn alloys transforms from coarse columnar grains to fine equiaxed grains after applying the vibration field. The MV enhances the solid solubility of Sn in the matrix and significantly refining grain size. Moreover, it optimizes the distribution and morphology of secondary phases while effectively suppressing micro-segregation. Performance tests show that increasing Sn content and applying mechanical vibration improve the hardness and tensile strength of the alloys, while the electrical conductivity is deteriorated. This research provides important guidance for the composition design and fabrication of Cu-Sn alloys with uniformly refined microstructures.

Cu-Sn alloy, as a typical Cu-based alloy with a history of thousands of years, is one of the oldest non-ferrous alloys[1]. The Sn element serves as the primary alloying element in Cu-Sn alloys, and its content exerts a crucial influence on the properties, including strength, corrosion resistance, and castability. These alloys find extensive applications in various industrial fields, including aviation, aerospace, electronics, machinery, automotive, and shipbuilding[2–6], where they are valued for their excellent wear resistance and good machinability characteristics.

During the solidification of metal melts, processes such as fluid flow, internal heat transfer, and solute redistribution have significant impact on the evolution of the microstructure. The complex interaction between thermal gradients, constitutional undercooling, and interface stability governs the microstructure evolution and defect formation. The control of these processes is closely related to the quality of ingots, making the regulation of solidification processes a persistent research focus in metallurgy[7]. Engineering-grade Cu-Sn alloys exhibit a wide crystallization temperature range and demonstrate mushy solidification characteristics, which present particular challenges for microstructural control. Under gravity casting conditions, defects such as shrinkage porosity, microporosity, and dendritic segregation are prone to appear, significantly impairing their mechanical properties and limiting their application in critical components. Furthermore, Cu-Sn alloys often develop coarse grains and large columnar grain ratios during conventional casting processes, leading to degraded performance and susceptibility to hot tearing during subsequent hot working[8–11]. The strong tendency for inverse segregation in these alloys further complicates the production of homogeneous microstructures, particularly in heavy sections.

Refining the grain size can effectively enhance the mechanical properties of Cu-Sn alloys through the well-established Hall-Petch effect. The application of external field treatments, such as mechanical vibration (MV), electromagnetic fields, and ultrasound vibration, have shown unique advantages in the casting process, thereby attracting a great deal of researches and practical applications[12–16]. Electromagnetic fields, in particular, have demonstrated remarkable capabilities in controlling solidification microstructures through Lorentz force-induced melt convection, which enhances heat and mass transfer, promotes dendrite fragmentation, and facilitates the transition from columnar to equiaxed grain growth[17,18]. Ultrasound vibration, another effective external field approach, generates both acoustic streaming and cavitation effects in the molten metal[19]. The acoustic streaming significantly improves mass and heat transfer during solidification, while the cavitation effect produces extreme localized pressures and temperatures that significantly increase nucleation rates and promote dendrite fragmentation[20,21]. MV primarily influences solidification through forced convection

[1] *Key Laboratory of Solidification Control and Digital Preparatiom Technology (Liaoning Province), School of Materials Science and Engineering, Dalian University of Technology, Dalian 116024, China*

[2] *China Railway Self-Creation Electric Co., Ltd 252000, China*

[3] *Ningbo Institute of Dalian University of Technology, Ningbo 315000, China*

* Corresponding author, E-mail: pbdut@dlut.edu.cn; jiejc@dlut.edu.cn

Received 29 October 2025; Accepted 14 December 2025; Published online 19 January 2026

DOI: 10.54227/mlab.20250103

and induced fluid flow, which effectively breaks developing dendrites and transports fragmented crystals throughout the melt, thereby creating additional nucleation sites. These advanced solidification control techniques can effectively manipulate fluid flow, temperature distribution, and crystal nucleation. Among these, MV has garnered widespread attention from researchers owing to its simple equipment requirements, significant grain refinement effects, and economic/environmental advantages[22,23]. While electromagnetic fields and ultrasonic vibration generally provides more intensive refinement effect, MV offers superior scalability for industrial applications with less complex implementation requirements, making it particularly suitable for large-scale casting processes where cost-effectiveness and operational simplicity are paramount considerations.

The non-contact nature of vibration treatment enables effective microstructural control while maintaining the compositional purity of the alloy. Current research on the influence of MV on alloy solidification primarily focuses on Al and Mg alloys[24–32], where it has been demonstrated to reduce grain size, improve mechanical properties, and reduce casting defects. However, studies reporting the application of external fields in Cu-Sn alloy solidification remain scarce, warranting further exploration. The unique solidification characteristics of Cu-Sn alloys, including their wide freezing range and strong segregation tendency, may respond differently to vibration treatment compared to lighter alloys. Therefore, in this investigation, Cu-*x*Sn (where x = 5 and 10 wt%) alloys were selected as research subjects, preparing alloy ingots with and without MV. The effect of MV on microstructure evolution is systematically examined, and the comprehensive property evaluations including hardness, tensile strength, and conductivity measurements are conducted to establish processing-structure-property relationships.

Experimental procedure

Experimental materials and process

The Cu-*x*Sn alloys were prepared using medium-frequency induction heating furnace. Electrolytic Cu and high-purity Sn blocks were placed in a graphite crucible and heated to be molten. The alloy melt was maintained at 1200 °C for 3 min to ensure homogeneity before casting. Cu-Sn samples were cast under MV, and Fig. 1 illustrates the schematic diagram of the experimental setup. The MV system comprises a three-phase asynchronous vibration motor, frequency converter, mold fastening device, and supporting frame. The graphite crucible, mounted on the MV platform, was preheated to 600°C in a muffle furnace (SX2-5-12). The molten alloy was then poured into the crucible. MV with a frequency of 30 Hz and amplitude of 2 mm was applied until complete solidification. The cast samples were subjected to subsequent machining to obtain the required specimens for further characterization.

Microstructure characterization

The chemical composition of the Cu-*x*Sn alloys was first analyzed using an X-ray fluorescence spectrometer (XRF, XRF-1800, Shimadzu), with the results summarized in Table 1. The phase composition of the Cu-Sn alloys was examined by X-ray diffractometer (XRD, D8 ADVANCE, Bruker). For microstructure observation, the samples were etched with $FeCl_3$ solution (5 g $FeCl_3$ + 5 mL HCl + 95 mL C_2H_5OH). The microstructure and surface morphology of the Cu-*x*Sn alloys were characterized using field-emission scanning electron microscope (SEM, SU5000, Hitachi). Additionally, electron probe microanalyzer (EPMA, JXA-8530F Plus, JEOL) was employed to conduct qualitative and quantitative analysis of selected regions.

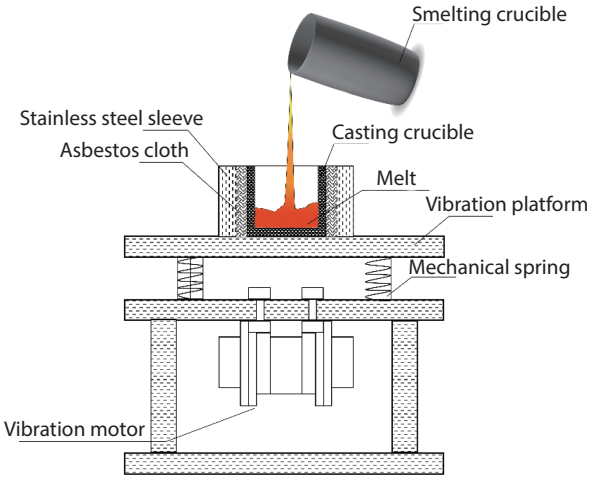

Fig. 1 Schematic diagram of the casting devices under MV

Table 1. Chemical composition of Cu-*x*Sn alloy under different conditions

Element	Cu (wt.%)	Sn (wt.%)
Cu-5Sn	95.11	4.89
MV Cu-5Sn	94.94	5.06
Cu-10Sn	90.24	9.76
MV Cu-10Sn	90.18	9.82

Properties tests

The hardness of the samples was measured using a Brinell hardness tester (HB-62.5MP, SIOMM). A ball indenter with diameter of 2.5 mm was adopted with load of 15.6 kgf and dwell time of 15 s. Measurements were taken with intervals of 0.5 mm, with at least five tests performed for each sample. The average value was adopted as the result. The electrical conductivity was evaluated at room temperature using a conductivity tester (Sigmascope SMP 350, Helmut Fischer). Each specimen was measured for five times, and the average value was calculated. The obtained conductivity values are reported in percentage of the International Annealed Copper Standard (%IACS). Room-temperature tensile tests were conducted on an electronic universal testing machine (UTM5000, SUNS) at a constant tensile speed of 0.3 mm/min. For each casting condition, a minimum of three specimens were collected from identical locations of the ingot and subsequently tested to ensure experimental consistency. Fracture surface morphology was subsequently examined using SEM to analyze the failure mechanisms.

Results and discussions

Microstructures of the as-cast Cu–*x*Sn alloys

The XRD patterns of the Cu-*x*Sn alloy are presented

DOI: 10.54227/mlab.20250103

inFig.2a. The diffraction analysis reveals that the phase composition of the Cu-*x*Sn alloys consists mainly of Sn-rich secondary phases and α-Cu solid solution. This observation clearly demonstrates that the application of MV during solidification does not lead to the formation of new precipitates. Significant differences in diffraction peak intensities were observed between vibrated and non-vibrated samples, indicating that MV treatment altered the crystallographic orientation of the alloys. Notably, the diffraction peaks exhibit apparent shifts after MV treatment as shown in Fig.2b, which provides direct evidence that MV enhances the solid solubility of Sn in the Cu matrix.

Fig.2c shows the macroscopic solidification morphology of Cu-*x*Sn alloys with different Sn contents and process conditions. The macroscopic structure of Cu-*x*Sn alloys consists of coarse columnar crystals without MV. After MV is applied, a large number of fine equiaxed crystals appear throughout the ingot cross-section, indicating that MV has significant grain refinement effect on Cu-Sn alloys. This is attributed to the convective motion induced by MV in the molten alloy, which promotes dendrite fragmentation and facilitates the formation of larger equiaxed grain zones. When the Sn content increases to 10 %, the grain size decreases significantly without MV application, although some coarse columnar or blocky crystals remain. This demonstrates that the solute Sn can refine the grain of Cu-Sn alloys under conventional conditions, while the solidification structure remains coarse. In fact, the interaction between Sn and Cu atoms in the alloy melt is also an important factor affecting grain size[33]. Adding Sn elements causes lattice distortion in Cu-Sn alloys, resulting in elevated grain boundary energy that facilitates grain refinement. These high-energy solute Sn elements tend to segregate at grain boundaries, thus inhibiting grain growth of Cu-Sn alloys.

Fig.3a-d show SEM images of the microstructures of Cu-5Sn and Cu-10Sn alloys under different conditions. The solidification microstructure mainly consists of dark gray primary Cu-rich phase and silver-white δ precipitates. The primary α-Cu phase occupies higher proportion in Fig.3a, c , exhibiting relatively coarse dendritic morphology with well-developed secondary dendrites. Most dendrites in the microstructure are fragmented after applying MV, the primary α-Cu phase is significantly refined, and equiaxed structures can also be found (Fig.3b, d). The morphology of the second phase changes from coarse needle-like/blocky shapes to fine particulate forms, showing dispersed distribution, indicating that MV treatment has a remarkable refinement effect on the solidification structure of Cu-Sn alloys as shown in Fig.3c-d. After MV treatment, the α-Cu dendrites transform from original network structures to discontinuous and dispersed skeletal morphology (Fig. 3b). The application of MV breaks the network distribution of intergranular precipitates in Cu-Sn alloys, thereby improving the overall mechanical properties.

To better characterize the effect of MV on elemental distribution, Fig.3e-f present the EPMA results to compare the microstructures of Cu-5Sn alloys processed with and without MV. Analysis of Fig.3e-f indicates three distinct compositional regions: the α-Cu matrix showing minimal Sn content, second phases with maximum Sn concentration, and intermediate transition zones between them. Notably, significant Sn enrichment is observed at α-Cu grain boundary regions, with substantially more pronounced segregation in non-vibrated samples compared to the vibrated samples. This demonstrates that MV effectively alleviates micro-segregation during solidification. Under non-equilibrium solidification conditions, the rapid cooling rate of the alloy melt prevents Sn atoms from diffusing into the α-Cu matrix, causing them to remain at grain boundary gaps and ultimately leading to the

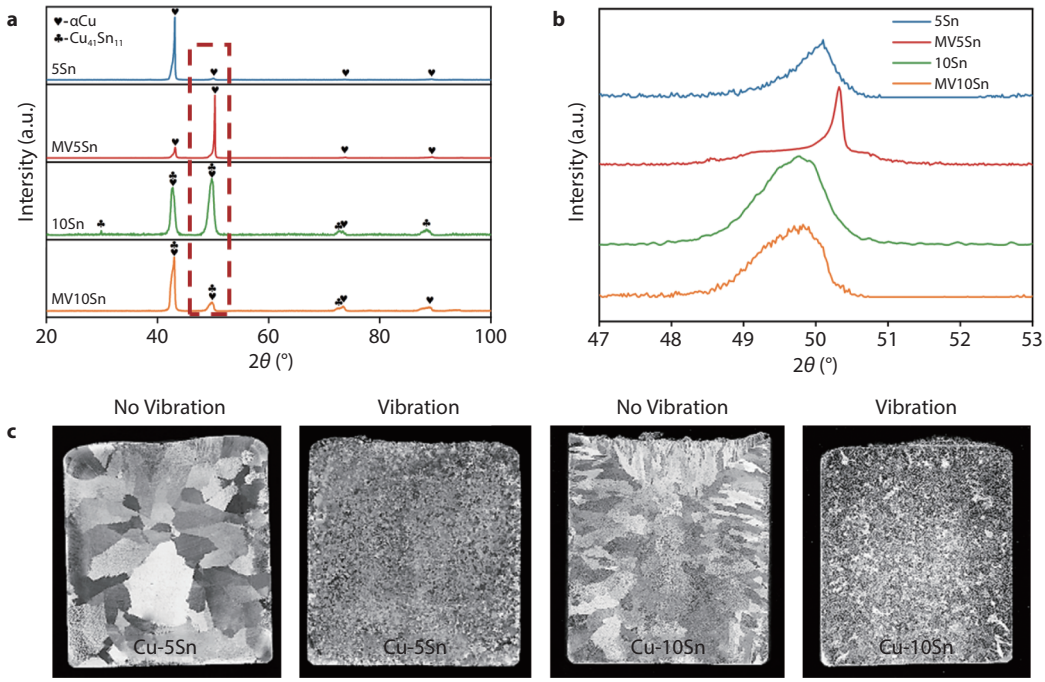

Fig. 2 **a** XRD results of Cu-*x*Sn alloy under different conditions, **b** partial enlarged images of the red dotted frame in **a**, **c** macroscopic structure of Cu-*x*Sn alloy under different conditions

DOI: 10.54227/mlab.20250103

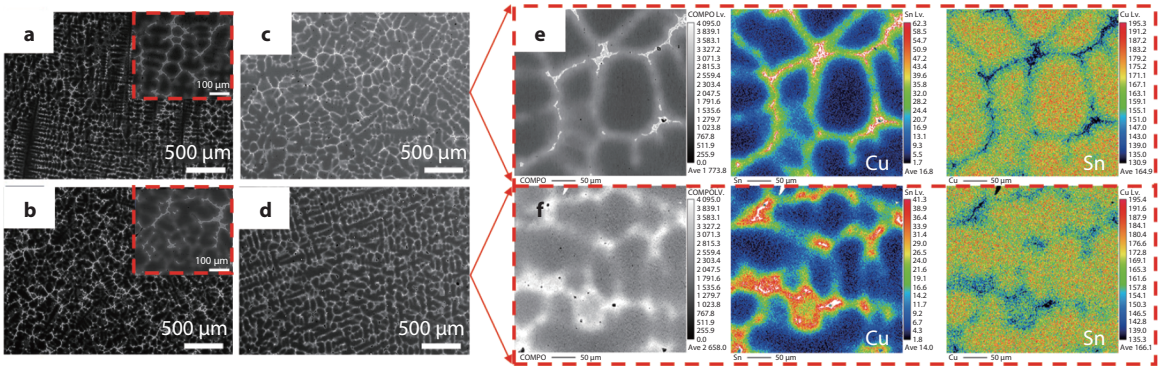

Fig. 3 The microstructure of Cu-*x*Sn alloys under different conditions: SEM of **a** Cu-10Sn without MV, **b** Cu-10Sn under MV, **c** Cu-5Sn without MV, **d** Cu-5Sn under MV, and corresponding EPMA of **e** Cu-5Sn without MV, **f** Cu-5Sn under MV.

formation of Sn-rich regions at these boundaries[34]. However, the presence of MV increases the number of disordered atoms in the molten alloy and enhances the diffusion ability of Sn elements, thereby inhibiting its segregation.

Properties of the as-cast Cu–*x*Sn alloys

Fig.4a presents the statistical distribution of Brinell hardness for Cu-*x*Sn alloy specimens under different conditions. The results demonstrate that hardness increases with increasing Sn content. Notably, at equivalent compositions, the specimens with MV exhibited superior hardness compared to their non-vibrated condition. This enhancement in hardness can be attributed to two primary strengthening mechanisms: first, the addition of Sn promotes substantial grain refinement through constitutional supercooling effects, which increases the density of grain boundaries and enhances strength according to the Hall-Petch relationship; second, a higher Sn content facilitates the precipitation of fine intermetallic phases, resulting in considerable precipitation strengthening through Orowan dislocation pinning mechanisms. The superimposed effect of mechanical vibration further intensifies these mechanisms by promoting more uniform solute distribution and increasing nucleation sites for precipitation. The electrical conductivity of Cu-*x*Sn alloys under different processing conditions is summarized in Fig.4b. The results show consistent degradation with increasing Sn concentrations. Furthermore, at 5% Sn content, the specimens under MV exhibit approximately 21% lower electrical conductivity than those processed without vibration. According to Matthiessen rule[35], solute atoms exert substantially greater influence on electron scattering than second-phase particles in Cu alloy systems. The progressive Sn addition leads to supersaturated solid solutions, where the atomic radius mismatch between Cu (0.128 nm) and Sn (0.158 nm) creates pronounced lattice distortion, thereby intensifying electron scattering and reducing conductivity. The MV promotes a more uniform distribution of Sn atoms within the matrix and increases dislocation density, further exacerbating the degree of lattice distortion and introducing additional scattering centers. These synergistic effects lead to the lower conductivity observed in the vibrated specimens. At the 10% Sn content, the influence of mechanical vibration on electrical conductivity was substantially reduced compared to its effects in low tin alloys, resulting in negligible variation in conductivity measurements.

Fig.5a shows the stress-strain curves of Cu-*x*Sn alloy specimens with and without MV. Table 2 presents the ultimate tensile strength (UTS) and corresponding elongation. It can be observed that the UTS is improved significantly as the Sn content increases. Specifically, at 5% Sn content, the specimens under MV achieved approximately 58% higher UTS and 37% greater elongation compared to their non-vibrated sample. This strengthening effect remained substantial at 10% Sn content, where the specimens under MV showed about 56% improvement in UTS and a remarkable 116% enhancement in elongation. These findings indicate that mechanical vibration effectively refines the alloy microstructure

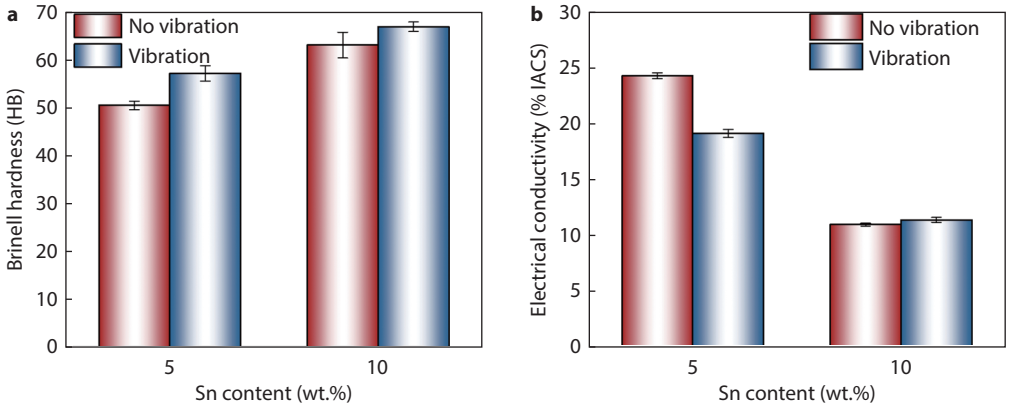

Fig. 4 **a** Hardness variation and **b** electrical conductivity of Cu-*x*Sn alloys under different conditions

DOI: 10.54227/mlab.20250103

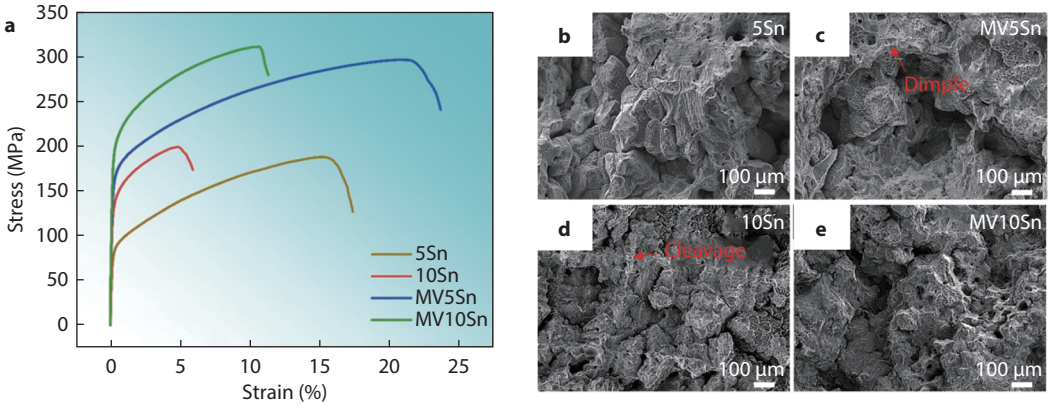

Fig. 5 Tensile properties of Cu-*x*Sn alloys under different conditions and corresponding tensile fracture microstructure, **a** stress-strain curves, tensile fracture microstructure of **b** Cu-5Sn, **c** MV Cu-5Sn, **d** Cu-10Sn and **e** MV Cu-10Sn

Table 2. Statistical results of tensile strength and elongation of Cu-*x*Sn

Specimens	Cu-5Sn	Cu-10Sn	MV Cu-5Sn	MV Cu-10Sn
UTS (MPa)	187	198	295	310
Elongation (%)	15.2	4.9	20.8	10.6

through dendrite fragmentation and enhanced nucleation, leading to simultaneous improvement in both strength and plasticity according to the Hall-Petch relationship. Furthermore, the exceptionally high strength observed in the Cu-10Sn alloy can also be attributed to the increased number of intergranular hard precipitations.

Fig.5b-e presents SEM images of fracture surfaces of Cu-*x*Sn tensile specimens. As shown in Fig.5b, d, the fracture morphology of Cu-*x*Sn alloy without MV exhibits brittle fracture characteristics with cleavage edges, which can be attributed to the distinct network microstructure of precipitates. The continuous network structure surrounding dendrites hinders matrix deformation and dislocation slip during tensile tests. Consequently, the fracture path preferentially follows these network precipitates, exhibiting brittle fracture characteristics and poor ductility.

Fig.5c shows the fracture surface of MV-treated Cu-5Sn, displaying numerous deep dimples. In the matrix, the uniformly dispersed precipitates facilitate initial dimples nucleation. These dimples gradually grow and coalesce with increasing deformation, ultimately leading to macroscopic fracture. Due to their small size, these precipitates provide limited obstruction to plastic flow and dislocation slip, thereby contributing to larger elongation.

Based on the experimental results, it is evident that MV can significantly improve the solidification microstructure of Cu-Sn alloys. The MV induces relative motion between liquid and solid phases during solidification, generating viscous resistance and shear forces[36–37], which break the well-developed network structures effectively. The viscous resistance serves as the fundamental cause of dendrite fragmentation. When analyzing the stress and fracture conditions of an individual dendrite under ideal conditions, the dendrite exists in a non-inertial system subject to three primary forces: excitation force, motion resistance, and inertial force. When these forces reach equilibrium, the dendrite remains stationary. The combined bending stress (σ_{com}) at the dendrite root cross-section can be calculated using Eq. (1):

$$\sigma_{com} = \sigma_{ZU(L)} + \sigma_{\alpha(L)} = \frac{240\eta L^2}{D_r^3} V + \frac{4\rho L^2}{D_r} \quad (1)$$

where η is the melt viscosity; L is the dendrite vibration length; Dr is the dendrite radius; V is the melt flow velocity; ρ is the dendrite density; α is the dendrite motion acceleration; $\sigma_{ZU(L)}$ is the viscous stress; $\sigma_{\alpha(L)}$ is the inertial stress. MV significantly increases both the melt flow velocity (V) and dendrite acceleration (α), thereby enhancing the combined bending stress on dendrites. When the bending stress at any dendrite cross-section exceeds its ultimate strength, dendrite growth is disrupted, leading to shear fracture. The fragmented dendrites are subsequently dispersed throughout the alloy melt under MV stirring, promoting multiplication, increasing nucleation rates while suppressing free dendrite growth, ultimately resulting in grain refinement of the Cu-Sn alloy.

To further investigate the influence of MV on the solidification behavior of Cu–Sn alloys, two K-type thermocouples were installed 40 mm above the bottom of the mold, one adjacent to the inner mold wall and the other at the center of the melt cavity. The cooling curves of Cu–5Sn alloy solidification with and without MV were compared. As shown in Fig.6 a-b, noticeable differences in cooling rates were observed under different MV conditions. In the absence of MV, the cooling rates measured at the center and the edge of the melt were 29.3 K/s and 36.6 K/s, respectively. Upon application of MV, the cooling rates increased to 36.6 K/s at the center and 61 K/s at the edge, indicating that MV significantly enhances the solidification rate of the melt. Moreover, the solidification time interval between the edge and center of the casting exhibited no marked difference under the two experimental conditions, even though previous studies have indicated that physical fields can enhance thermal homogenization within the liquid zone[38–41]. Although the mold was preheated, the relatively high melting point of the Cu–Sn alloy, the limited mold diameter, and the thin insulation layer collectively resulted in negligible differences in cooling rates between the edge and center regions, both with and without MV.

As schematically illustrated in Fig. 6c-d, the mechanisms of

DOI: 10.54227/mlab.20250103

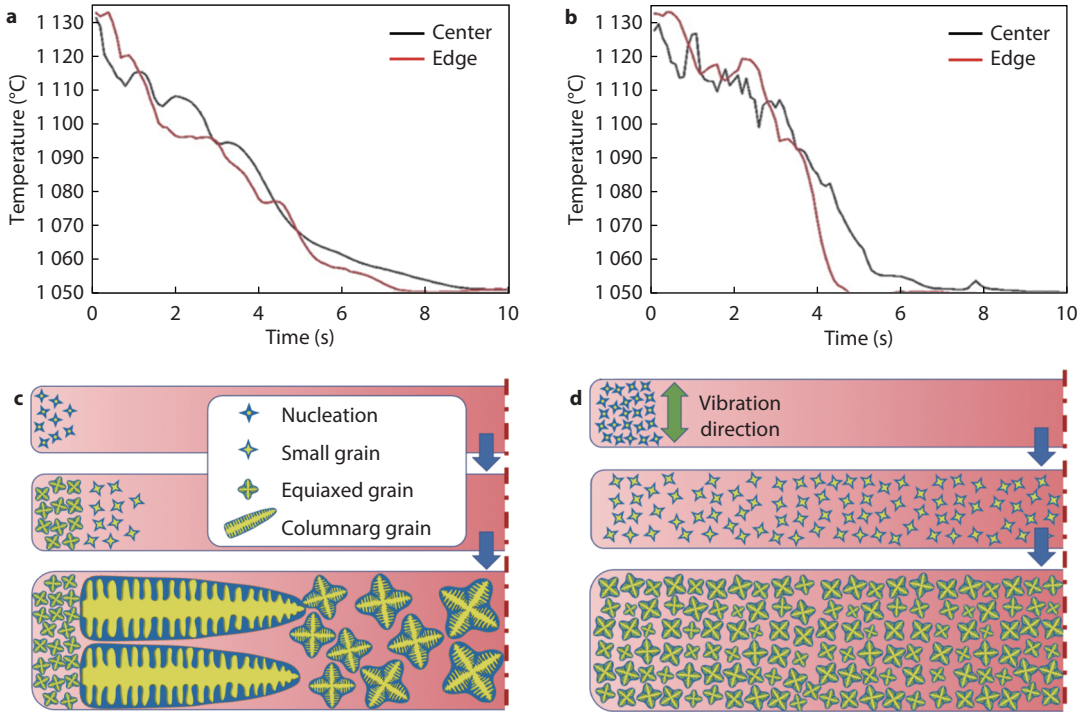

Fig. 6 The cooling curves of Cu–5Sn alloy **a** without and **b** with MV, schematic diagram of grain formation and growth **c** without and **d** with MV

grain formation and growth under different solidification conditions are compared. Without MV, the solidification structure exhibited characteristic features, including a chill zone, columnar grain zone, and central equiaxed grain zone. The grains were relatively coarse, which can be attributed to a low nucleation rate and a broad solidification interval. In contrast, MV applies shear stress to growing columnar dendrites, leading to their fragmentation and generating additional nucleation sites. The induced forced convection further contributes to a uniform temperature distribution and enhanced cooling rate, thereby increasing the nucleation rate. Consequently, under MV stirring, the nucleated particles become uniformly dispersed throughout the melt, resulting in a refined and homogeneous equiaxed grain structure.

Conclusion

This study investigated the effects of mechanical vibration (MV) on the solidification microstructure and properties of Cu-*x*Sn alloys, and elucidates the underlying mechanisms, yielding the following conclusions:

(1) MV enhances the solid solubility of Sn in the matrix, significantly refines grain structure, and improves the distribution, morphology, and micro-segregation of precipitates.

(2) Both increasing Sn content and applying MV improve hardness and tensile strength, while reduce electrical conductivity. MV enhances both strength and ductility, while higher Sn content decreases ductility. Fractographic analysis shows MV facilitates a transition from brittle to ductile fracture modes.

(3) Vibration-induced stirring increases the cooling rate, thereby enhancing the nucleation rate. Vibration simultaneously suppresses the growth of small grains and fragments columnar crystals, promoting their uniform dispersion within the melt.

Acknowledgements

The authors gratefully acknowledge the supports of Natural Science Foundation of China (Nos. U23A20611, 52501041), Science and Technology Innovation Project of Ningbo (Nos. 2024Z077, 2023Z100), China Postdoctoral Science Foundation (Nos. 2024M750312, GZB20240091), Liaoning Province Doctoral Research Start-up Fund Program Project (No. 2025-BS-0043).

REFERENCES

1. D. Li, P. Franke, S. Fürtauer, D. Cupid, H. Flandorfer, *Intermetallics*, 2013, 34, 148
2. K. Chen, X. Wu, A. Zhang, J. Zhang, X. Chen, Y. Zhu, Z. Wang, *Appl. Surf. Sci.*, 2022, 573, 151623
3. Q. Lei, Z. Li, T. Xiao, Y. Pang, Z. Q. Xiang, W. T. Qiu, Z. Xiao, *Intermetallics*, 2013, 42, 77
4. Z. Guo, J. Jie, S. Liu, J. Liu, S. Yue, Y. Zhang, T. J. Li, *Metall. Mater. Trans. A*, 2020, 51, 1229
5. J. Stella, L. Gerke, M. Pohl, *Wear*, 2013, 303, 541
6. Moharami, Ali, *J. Mater. Res. Technol.*, 2020, 9, 10091
7. W. Low, M. Schieber, Applied Solid State Physics. Springer, New York, 1970, pp 161–170
8. B. Dong, J. C. Jie, X. X. Yao, S. C. Liu, Y. H. Chen, N. Zhong, T. J. Li, *J. Alloys Compd.*, 2019, 791, 936
9. C. Paul, R. Sellamuthu, *Procedia Eng.*, 2014, 97, 1341
10. X. Du, F. Wang, Z. Wang, L. Zhou, Z. Wei, Z. Liu, P. Mao, *J. Alloys Compd.*, 2022, 911, 165113
11. J. Hui, Z. Feng, W. Fan, X. Yuan, *Mater. Charact.*, 2018, 144, 611
12. Yu. M. Gelfgat, *J. Cryst. Growth*, 1999, 198, 165
13. Z. Guo, J. Jie, S. Yue, T. Li, Q. Guo, *Mater. Sci. Eng.*, 2018, 424, 12073

DOI: 10.54227/mlab.20250103

14. Z. Xu, H. Liu, L. Li, C. Sun, X. Tan, B. Chen, Q. Dong, Y. Wu, J. Jiang, J. Ma, *Acta Metall. Sin.*, 2024, 7, 1135
15. J. Luo, H. Luo, C. Liu, T. Zhao, R. Wang, Y. Ma, *Mater. Sci. Eng. A*, 2020, 798, 139990
16. H. R. Kotadia, M. Qian, D. G. Eskin, A. Das, *Mater. Des.*, 2017, 132, 266
17. Z. Yan, Z. Shi, J. Xie, Y. Teng, *Mater. Sci. Eng. A*, 2022, 856, 143985
18. J. Jie, S. Yue, J. Liu, D. H. Sthohn, Y. Zhang, E. Guo, T. Wang, T. Li, *Acta Mater.*, 2021, 208, 116747
19. S. Wang, D. Chen, X. Zhang, Q. Wang, R. Chen, *Int. J. Heat Mass Tran.*, 2024, 221, 125032
20. A. Li, R. Jiang, R. Li, A. Fu, L. Zhang, L. Zhang, *Ultrason. Sonochem.*, 2025, 117, 107341
21. J. Cai, L. Zhang, L. Li, G. Lu, C. Xu, R. Jiang, Y. Zhang, L. Wu, S. Guan, *J. Mater. Res. Technol.*, 2025, 36, 2053
22. K. Kocatepe, C. F. Burdett, *J. Mater. Sci.*, 2000, 35, 3327
23. V. Chaturvedi, T. Talapaneni, *J. Mater. Eng. Perform.*, 2021, 30, 3187
24. W. Jiang, X. Chen, B. Wang, Z. Fan, H. Wu, *Int. J. Adv. Manuf. Technol.*, 2016, 83, 167
25. T. Tamura, T. Matsuki, K. Miwa, *Mater. Trans.*, 2011, 52, 830
26. C. Sui, Z. Liu, X. Ai, C. Liu, Z. Zou, *Crystals*, 2022, 12, 240
27. Y. Zheng, L. Ding, H. Ye, Z. Chen, *Nanoscale Res. Lett.*, 2017, 12, 308
28. M. Li, T. Tamura, *J. Alloys Compd.*, 2021, 883, 160915
29. W. Jiang, Z. Fan, X. Chen, B. Wang, H. Wu, *Mater. Sci. Eng. A*, 2014, 619, 228
30. V. Chaturvedi, A. Sharma, U. Pandel, *Mater. Res. Express*, 2017, 4, 046501
31. B. Lin, X. He, S. Xia, H. Xiao, Y. Zhao, K. Khanlari, *Trans. Nonferr. Met. Soc. China.*, 2024, 34, 2393
32. J. Chen, X. Chen, Z. Luo, *Results Phys.*, 2018, 11, 1022
33. L. Zhang, Y. Li, R. Zhou, X. Wang, Q. Wang, L. Xie, Z. Li, B. Xu, *Crystals*, 2023, 13, 1532
34. T. Zheng, B. Zhou, J. Wang, S. Shuai, Y. Zhong, W. Ren, Z. Ren, F. Debray, E. Beaugnon, *Mater. Sci. Eng. A*, 2018, 733, 170
35. M. R. Islam, P. Karna, J. A. Tomko, E. R. Hoglund, D. M. Hirt, M. S. B. Hoque, S. Zare, K. Aryana, T. W. Pfeifer, C. Jezewski, A. Giri, C. D. Landon, S. W. King, P. E. Hopkins, *Nat. Commun.*, 2024, 15, 9167
36. Q. Lin, Z. Zhang, B. Guo, W. Li, J. Mi, *Acta Metall. Sin.*, 2023, 36, 857
37. S. Gencalp, N. Saklakoglu, *Arab. J. Sci. Eng.*, 2012, 37, 2255
38. Z. Zhao, Y. Liu, L. Liu, *Mater. Manuf. Processes*, 2024, 166, 108196
39. F. Taghavi, H. Saghafian, Y. Kharrazi, *Mater. Des.*, 2009, 30, 1604
40. R. M. Pillai, K. S. Kumar, B. C. Pai, J, *Mater. Process. Tech.*, 2004, 146, 338
41. J. Yao, S. Fan, X. Liu, X. Ding, H. Huang, W. Wu, Q. Wang, L. Wang, Y. Su, *Mater. Sci. Eng. A*, 2023, 865, 144630